Pergamon

Int. J. Heat Mass Transfer. Vol. 41, No. 15, pp. 2383–2397, 1998
© 1998 Elsevier Science Ltd. All rights reserved
Printed in Great Britain
0017–9310/98 $19.00+0.00

PII: S0017–9310(97)00300–1

Frictional losses and convective heat transfer in sparse, periodic cylinder arrays in cross flow

A. R. MARTIN
Department of Mechanical Engineering, University of Florida, Gainesville, FL 32611, U.S.A.

C. SALTIEL†
Synergetic Technologies, Inc., Delmar, NY 12054, U.S.A.

and

W. SHYY
Department of Aerospace Engineering, Mechanics and Engineering Science, University of Florida, Gainesville, FL 32611, U.S.A.

(*Received* 13 *May* 1997 *and in final form* 24 *September* 1997)

Abstract—A numerical study of fluid flow and heat transfer around periodic cylinder arrays under laminar cross flow conditions is presented. The investigation considers flow in sparse square and triangular arrays, with fluid fractions ranging from 0.80–0.99 and particle Reynolds numbers from about 3–160. Volume averaging of the microscopic flow field variables is used to ascertain the functional form of coefficients appearing in the macroscopic (porous media) equations. Frictional losses are shown to follow Darcy's law when the Darcian Reynolds number is of the order of one, while significant non-Darcy effects are seen at higher Reynolds numbers. The validity of the Forchheimer and Ergun correlations is shown to be suspect for flow in this highly porous media. Local thermodynamic equilibrium is relaxed in order to explore cylinder-to-fluid convective heat transfer. Power-law relationships for frictional losses and Nusselt number are shown to correlate well with detailed simulation results. © 1998 Elsevier Science Ltd. All rights reserved.

1. INTRODUCTION

The flow of fluids through cylinder arrays is important in a multitude of applications, such as filtration, biological systems, and heat exchangers. Cross flow in periodic cylinder arrays has been the focus of a large number of investigations; review articles by Åström *et al.* [1] and Žukauskas [2, 3] list over 300 references related to flows in fibrous media and tube bundles, respectively. Despite this wealth of information, questions remain concerning the quantitative nature of flow in high porosity cylinder arrays: treating the cylinder array as a porous media, can flow be considered Darcian and, if not, can other simplifying procedures be used to approximate the flow stream. For the case of flows in sparse, periodic arrays, where the spacing to diameter ratio c/d is greater than two, previous studies have investigated creeping flow conditions alone, such as Drummond and Tahir [4] and Sangani and Acrivos [5]. At higher Reynolds numbers, investigations of flows through cylinder arrays have been presented by Edwards *et al.* [6], Eidsath *et al.* [7], and Ghaddar [8], but these studies emphasized low porosity cases (less than 0.80). Investigations of sparse cylinder arrays under the conditions of high Reynolds number are warranted for a number of applications. For example, Im and Ahluwahlia [9] examined highly porous fiber arrays to enhance internal heat transfer inside tubes. Also, Hendricks *et al.* [10] experimentally investigated the use of brush inserts, which can be represented as a cylinder array, within a complex cooling passage for the mitigation of flow separation and augmentation of local heat transfer. For both of these applications, high porosities are desirable in order to minimize frictional losses. Moreover, because these situations feature developing or recirculating flows, there is a need to understand the flow resistance offered by sparse cylinder arrays in the transverse direction. Evaluation of the global-scale flow field in these circumstances thus involves microscopic modeling for the quantification of the arrays' flow resistance, which may then be recast in terms of porous media. This approach represents a valuable tool which may be used to assess the macroscopic effects of various cylinder arrangement and porosity scenarios.

Analysis of heat transfer between cylinders and fluid is also of importance in high porosity cylinder arrays.

† Author to whom correspondence should be addressed.

NOMENCLATURE

a	specific surface area
A	first Ergun constant
b	modified friction factor correlation constant
B	second Ergun constant
c	cylinder spacing
c_p	specific heat
C	constant
d	cylinder diameter
Da	Darcy number
f	modified friction factor
F	Forchheimer constant
g	Nusselt number correlation constant
h	convective heat transfer coefficient
k	thermal conductivity
$\mathbf{k}_{ef}$	effective thermal conductivity tensor
K	permeability
m	modified friction factor correlation constant
n	modified friction factor correlation constant
Nu_d	Nusselt number
p	pressure
q''	heat flux
r	Nusselt number correlation constant
Re_d	particle Reynolds number
$Re_{\sqrt{K}}$	Darcian Reynolds number
$\mathbf{S}_f$	interfacial momentum source term tensor
T	temperature
T_r	reference temperature
$\mathbf{u}$	velocity vector
v	velocity
V	representative elementary volume (REV).

Greek symbols

δ_m	maximum percent relative difference
ε	volume fraction
μ	dynamic viscosity
ρ	density
Φ	scalar or vector quantity.

Subscripts and superscripts

f	fluid phase
fs	fluid–solid interface
k	phase
s	solid phase
*	nondimensional quantity.

Nusselt number correlations are available for flows within tube bundles [2, 3, 11], but there is little data for flows in sparse arrays. In some circumstances, e.g., nuclear systems [12, 13], the assumption of local thermodynamic equilibrium (LTE) must be relaxed. (The condition of LTE presumes that all phases are isothermal within the representative elementary volume.) It is the combination of high porosity and significant internal heat generation, radiation, or transient effects which render the LTE assumption invalid. The two previously mentioned investigations [9, 10] fall into this category. Considering flows in dense cylinder arrays, temperature differences between cylinders and bulk fluid are minimal since the cylinder is in close contact with the fluid. In sparse arrays, however, cylinders are isolated from much of the fluid and significant temperature gradients within the fluid space may exist. Only at a distance downstream does the bulk fluid temperature catch up with the cylinder temperature; an entrance length which depends on the flow field and initial temperature differences. Evaluation of Nusselt number for such flows is required to assess the LTE assumption (for example, see Amiri and Vafai [12]).

The objective of the present study is to investigate laminar fluid flow and heat transfer transverse to square and triangular periodic arrays of cylinders with large spacing ratios. Specifically, fluid volume fractions ε_f range from 0.80–0.99, and the particle Reynolds numbers Re_d (where d is the cylinder diameter) vary from approximately 3–160. The macroscopic effects of the cylinder arrays are assessed by considering the arrays as a porous media, with coefficients appearing in the macroscopic equations determined by volume averaging of the microscopic flow field variables. Non-Darcian behavior is expected to play an important role due to the combination of large fluid volume fraction and high Reynolds number. Comparisons are made to the Ergun and Forchheimer relations to examine their validity in this porosity range. For the case of heat transfer, LTE is not assumed, and both constant wall temperature and constant wall heat flux conditions are investigated.

2. MICROSCOPIC AND MACROSCOPIC FLOW EQUATIONS

Before the cylinder array problem is introduced, it is instructive to summarize the development of the porous media flow equations via examination of the microscopic equations. Similar to the Reynolds averaging concept in the analysis of turbulent flow, volume averaging is used to simplify the complexities of flow in porous media [14]. The volume average of any

scalar or vector quantity Φ_k, associated with phase k, is defined as

$$\langle\Phi_k\rangle = \frac{1}{V}\int_V \Phi_k \, dV \tag{1}$$

where V is the representative elementary volume (REV). (Φ_k is zero in regions not occupied by phase k.) The intrinsic volume average is defined as

$$\langle\Phi_k\rangle^k = \frac{1}{V_k}\int_{V_k} \Phi_k \, dV \tag{2}$$

and may be related to the total volume average by $\varepsilon_k\langle\Phi_k\rangle^k = \langle\Phi_k\rangle$, where ε_k is the volume fraction of phase k. The porous media, or macroscopic, flow equations are derived by taking the volume average of the microscopic conservation equations of continuity, momentum, and energy:

$$\nabla\cdot\mathbf{u} = 0 \tag{3}$$

$$\rho\mathbf{u}\cdot\nabla\mathbf{u} = -\nabla p + \mu\nabla^2\mathbf{u} \tag{4}$$

$$\rho c_p \nabla\cdot T\mathbf{u} = k\nabla^2 T. \tag{5}$$

In the above expressions, $\mathbf{u}$ is the velocity vector, ρ is the density, p is the pressure, μ is the dynamic viscosity, c_p is the specific heat, and k is the thermal conductivity. The system described here consists of two phases, a single phase fluid and solid, each having constant properties and spatially uniform volume fractions; the solid is stationary with respect to the external reference frame; and the flow is laminar and steady.

After volume averaging, the macroscopic governing equations for the fluid phase are [12, 14, 15]

$$\nabla\cdot\langle\mathbf{u}_f\rangle = 0 \tag{6}$$

$$\frac{\rho_f}{\varepsilon_f^2}\langle\mathbf{u}_f\rangle\cdot\nabla\langle\mathbf{u}_f\rangle = -\nabla\langle p_f\rangle^f + \frac{\mu_f}{\varepsilon_f}\nabla^2\langle\mathbf{u}_f\rangle - \mathbf{S}_f \tag{7}$$

$$\rho_f c_{p,f}\nabla\cdot\langle T_f\rangle^f\langle\mathbf{u}_f\rangle = \mathbf{k}_{ef}\varepsilon_f\nabla^2\langle T_f\rangle^f + h_{fs}a_{fs}(\langle T_s\rangle^s - \langle T_f\rangle^f) \tag{8}$$

where $\mathbf{S}_f$ is the interfacial momentum source term tensor, $\mathbf{k}_{ef}$ the effective fluid thermal conductivity tensor, h_{fs} the interfacial convection coefficient, and a_{fs} the specific surface area of the interface. The treatment of $\mathbf{S}_f$ and h_{fs} for periodic cylinder arrays in cross flow is the focus of this study; see Bauer [16] for the treatment of conductivity in fibrous media.

The primary difficulty encountered in applying the macroscopic equations to a given problem is the specification of these additional source terms arising from the volume averaging operation (analogous to the closure problem in turbulence [17]). In considering the macroscopic momentum equation with negligible convection and diffusion, the pressure gradient $-\nabla\langle p_f\rangle^f$ of the porous media for uni-directional flow (and hence each component of $\mathbf{S}_f$) can be determined either by the Ergun equation [18],

$$-\nabla\langle p_f\rangle^f = A\frac{\varepsilon_f^2}{(1-\varepsilon_f)^3}\frac{\mu\langle v_f\rangle}{d_p^2} + B\frac{\varepsilon_f}{(1-\varepsilon_f)^3}\frac{\rho\langle v_f\rangle\cdot|\langle v_f\rangle|}{d_p} \tag{9}$$

or by the Forchheimer equation [12, 14, 19],

$$-\nabla\langle p_f\rangle^f = \frac{\mu\langle v_f\rangle}{K} + \frac{F\rho}{\sqrt{K}}\langle v_f\rangle\cdot|\langle v_f\rangle|. \tag{10}$$

In these equations, v_f is the fluid velocity in the streamwise direction, A and B are the first and second Ergun coefficients, F is the Forchheimer term, and K is the intrinsic or Darcian permeability (defined below). Although these two expressions have a slightly different form, each employs one term to handle low velocity situations (creeping flow) and a second term to include the effects of turbulence and/or inertia (hence the appearance of velocity squared). For cases where the fluid velocity is sufficiently small, the well-known Darcy's law [14, 19] is recovered from equations (9) and (10), i.e.

$$-\nabla\langle p_f\rangle^f = \frac{\mu\langle v_f\rangle}{K}. \tag{11}$$

The interfacial convection coefficient must be specified if the LTE assumption is relaxed, and its value may be determined from application of Newton's law of cooling,

$$q_s'' = h_{fs}(T_s - T_r) \tag{12}$$

where q_s'' is the convective heat flux and T_r the reference temperature.

Coefficients appearing in the Ergun and Forchheimer relationships, along with the specification of the heat transfer coefficient, traditionally have been determined by least squares fitting of data from flow experiments. More recently, numerical solutions of the microscopic flow field have been used to determine these macroscopic coefficients, as reported in a number of investigations for flows in various cylinder arrays [4–8]. This technique is adopted in the present study, which may be stated as follows: (1) determine the flow field via the microscopic equations; (2) compute the volume average of the flow field variables within the REV; and (3) evaluate the resulting macroscopic source terms as a function of array type, fluid volume fraction, and flow condition.

3. PROBLEM DESCRIPTION AND NUMERICAL APPROACH

Figure 1 shows square and triangular arrays of cylinders with diameter d and spacing c, with the flow oriented in the y coordinate direction. (Other flow directions are possible, of course, but the present analysis is limited to only a single transverse

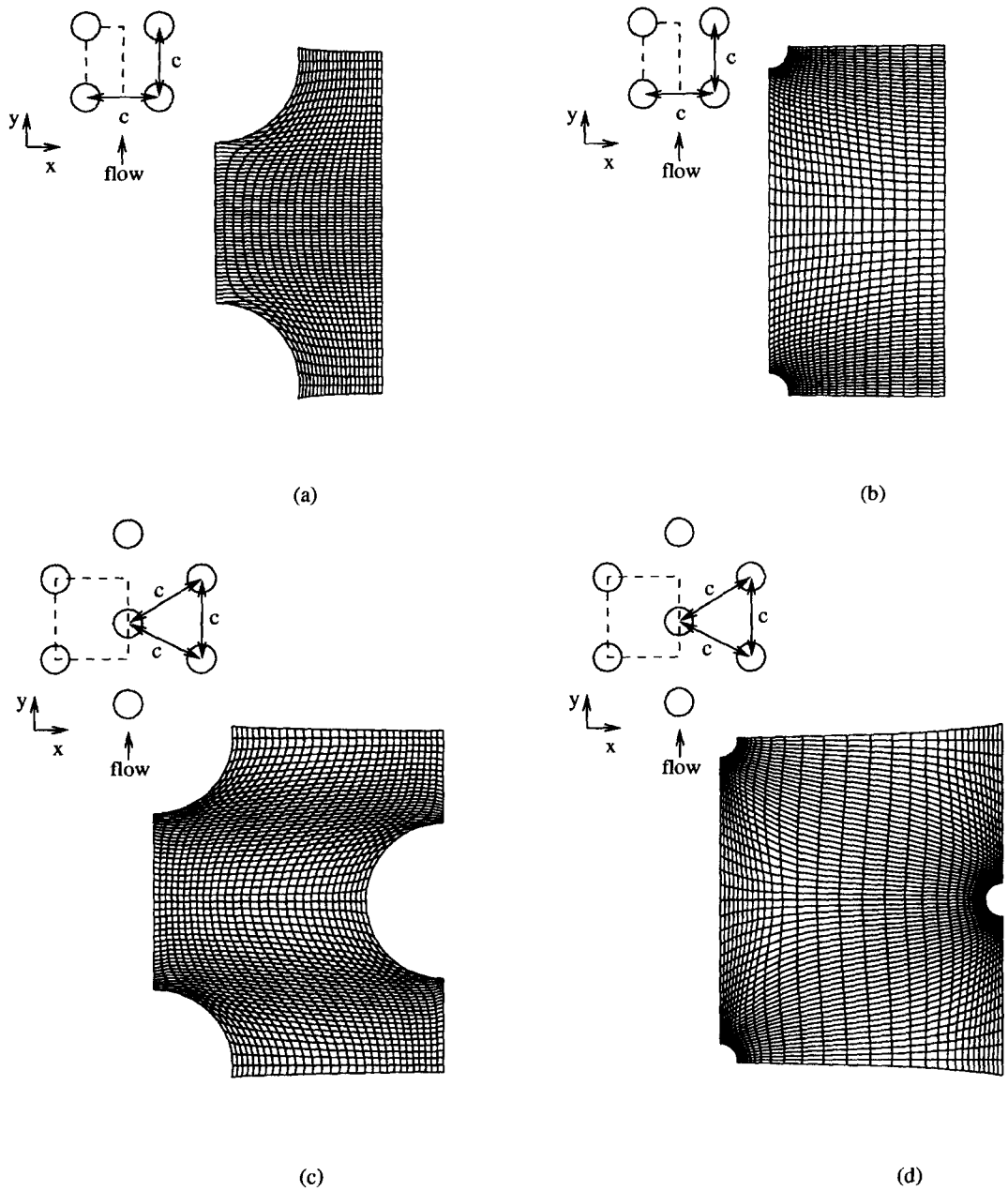

Fig. 1. Computational grids for cylinder arrays: (a) square array, $\varepsilon_f = 0.80$; (b) square array, $\varepsilon_f = 0.99$; (c) triangular array, $\varepsilon_f = 0.80$; (d) triangular array, $\varepsilon_f = 0.99$.

direction.) The cylinder spacing is fixed by specification of the fluid volume fraction ε_f, where

$$\varepsilon_f = 1 - \frac{\pi}{4}\left(\frac{c}{d}\right)^{-2} \tag{13}$$

for the square array, and

$$\varepsilon_f = 1 - \frac{\pi}{2\sqrt{3}}\left(\frac{c}{d}\right)^{-2} \tag{14}$$

for the triangular array. For the present study, ε_f ranges from 0.80 to 0.99 for each array, corresponding to c/d ratios from about two to ten. If entrance effects are negligible, which is a reasonable assumption for a cylinder array with a large number of rows, periodicity reduces the problem to the determination of velocity, pressure, and temperature fields in the fluid surrounding a solitary cylinder within the array. These flow domains are shown in Fig. 1 with dashed lines, which are taken to be the REV for volume averaging purposes (note that symmetry conditions are invoked for the square array).

A finite volume-based numerical procedure, as described by Thakur *et al.* [20] and Shyy [21], is uti-

Table 1. Grid sensitivity comparison for square array, $\varepsilon_f = 0.99$, $-\Delta p = 1.0$ N m^{-2}

Grid size	Re_d	$\lvert\delta_m\rvert$ (%)	$\log_{10}$ normalized residuals: x momentum	y momentum	Continuity
21×63	57.9	1.7	−5.3	−4.8	−5.3
41×63	58.3	1.0	−5.4	−4.6	−5.3
21×123	58.8	0.2	−5.0	−4.5	−5.0
41×123	58.9	—	−5.1	−4.2	−5.0

lized to solve the microscopic equations (3)–(5) in curvilinear coordinates for two-dimensional flow. This procedure is based on the SIMPLE algorithm [22] extended to curvilinear coordinates and employing mixed cartesian and contravariant velocity components, with a second order upwinding arrangement for convective terms. No-slip, no penetration boundary conditions are imposed at the cylinder surface, along with either constant temperature or constant heat flux boundary conditions. The inlet and outlet are periodic, with pressure difference $-\Delta p$ driving the flow. Treatment of the periodic boundary conditions in the context of a finite volume procedure is discussed in Patankar *et al.* [23]. Fluid surfaces not in contact with the cylinder are taken as symmetric and adiabatic.

The overall dimensions of the computational array are fixed by specifying ε_f and the cylinder diameter, which is 1.50×10^{-4} m (this is a representative size for a cylindrical fiber or wire); the cylinder length is set to unity (1.0 m). Figure 1 illustrates the typical grids used for square and triangular arrays for the extreme ε_f values, 0.80 and 0.99. A 21×63 grid is selected for the square array, while a 31×63 grid is chosen for the triangular array, which has a smaller aspect ratio. The grids are constructed to maximize the number of cells adjacent to solid surfaces, where sharp gradients in fluid velocity and temperature are expected. Overlapping grid cells are present at periodic inlet and outlet faces, and care is taken to ensure symmetric about the lateral centerline of the domain. Grid sensitivity was investigated for the square array with $\varepsilon_f = 0.99$ under high Reynolds number flow. Table 1 shows a comparison of the computed particle Reynolds number resulting from the pressure difference $-\Delta p = 1.0$ N m^{-2} for four different grid sizes: 21×63, 41×63, 21×123, and 41×123. Since the maximum relative difference δ_m between the finest grid and the coarser grid results is less than 2%, the solution was considered to be grid independent; hence the coarsest grid was selected to minimize computational effort. Normalized residuals are also included in Table 1, which are typical values obtained for all other cases. The solution of the continuity and momentum equations for each array required 4–6 h of CPU time on a middle-end workstation (DEC 3000 Model 600), with about 30 min for the solution of the energy equation.

Physical properties of the fluid are of air at 300 K: $\rho = 1.23$ kg m^{-3}; $\mu = 1.79 \times 10^{-5}$ N-s m^{-2}; $c_p = 1006$ J kg-K^{-1}; and $k = 0.025$ W m-K^{-1} [24]. Although any other fluid could have been selected, air is chosen to be representative of a gas flow (Prandtl number dependency is not considered in this work).

4. RESULTS: FLUID FLOW

To illustrate the qualitative features of the flow field, streamline plots are shown in Fig. 2 for the square array and Fig. 3 for the triangular array under low and high flow rate conditions. For small particle Reynolds numbers Re_d, where

$$Re_d = \frac{\rho \langle v_f \rangle d}{\mu} \tag{15}$$

a Stokes type of flow field can be seen, with little or no vortex generation behind the cylinders. As Re_d increases, the vortex behind the cylinder grows and extends up to the front of the downstream cylinder where $\varepsilon_f = 0.80$.

The presentation of the quantitative flow features now follows by treating Darcian and non-Darcian flow regimes individually.

4.1. *Darcian flow regime*

The Darcian Reynolds number, $Re_{\sqrt{K}}$, is often used as a criteria for determining the regime of flow through porous media:

$$Re_{\sqrt{K}} = \frac{\rho \langle v_f \rangle \sqrt{K}}{\mu}. \tag{16}$$

For $Re_{\sqrt{K}} < \mathcal{O}(1)$, Darcian flow holds [14], and the pressure drop in the flow direction is specified by equation (11). Hence, if the pressure drop and volume averaged streamwise velocity are known, the permeability K may be computed for a given array provided that $Re_{\sqrt{K}}$ is sufficiently small. In order to compute K from the present results, it is necessary to compute the pressure drop corresponding to $Re_{\sqrt{K}} = 0$ by linear extrapolation of the data, as the numerical procedure cannot handle flows at very low Reynolds numbers. To illustrate, Darcy's law may be written as

$$-\nabla \langle p_f \rangle^f \left(\frac{d^2}{\mu \langle v_f \rangle} \right) = \frac{d^2}{K} \tag{17}$$

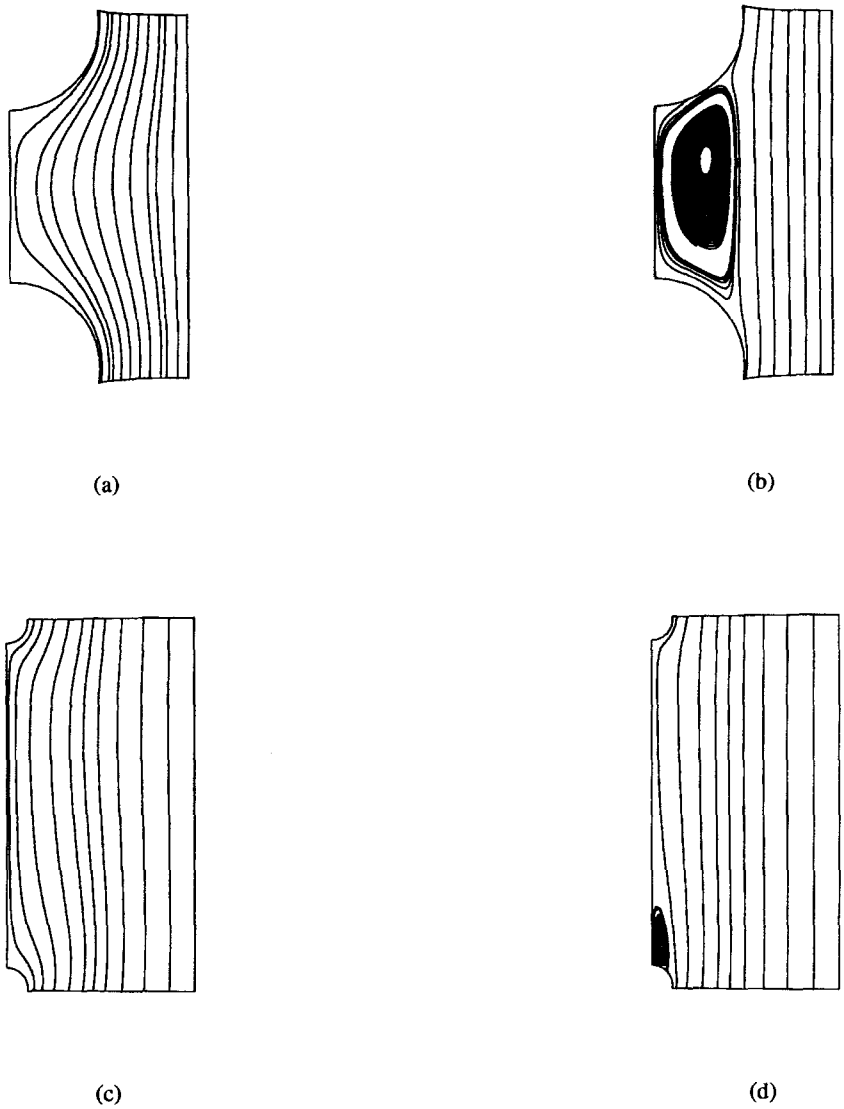

Fig. 2. Streamline plots for square array: (a) $\varepsilon_f = 0.80$, $Re_d = 3.26$ ($Re_{\sqrt{K}} = 0.904$); (b) $\varepsilon_f = 0.80$, $Re_d = 161$ ($Re_{\sqrt{K}} = 44.6$); (c) $\varepsilon_f = 0.99$, $Re_d = 4.24$ ($Re_{\sqrt{K}} = 13.3$); (d) $\varepsilon_f = 0.99$, $Re_d = 105$ ($Re_{\sqrt{K}} = 331$).

where the left-hand side of the above expression is defined as the nondimensional pressure gradient $(-\nabla p^*)$. The permeability for a given fluid volume fraction is found by computing $-\nabla p^*$ for data points 1 and 2 at low Reynolds number, and then extrapolating to $Re_d = 0$:

$$\frac{(-\nabla p^*)_2 - (-\nabla p^*)_1}{(Re_d)_2 - (Re_d)_1} = \frac{(-\nabla p^*)_1 - (-\nabla p^*)_0}{(Re_d)_1 - 0}. \quad (18)$$

Once $(-\nabla p^*)_0$ is computed, the permeability may be found from equation (17). Figure 4 shows a plot of the Darcy number, $Da = K/d^2$ vs. the fluid volume fraction for both array types. A comparison is made to the results of Drummond and Tahir [4], who conducted a Stokes flow analysis to obtain closed-form solutions for the permeability of various arrays (similar findings can be found in Sangani and Acrivos [5]). Since the fluid volume fraction is large, little difference can be seen between square and triangular array results. There is excellent agreement (less than 5% relative difference) between the current study and the Stokes flow solutions, which shows that the numerical procedure is accurate for the low Reynolds number range. Another implication of this comparison is that the present numerical procedure, which has significant numerical dissipation in the creeping flow regime, can be used to compute permeability to a high degree of accuracy. Thus, future studies of flows in other types of porous media could use computational fluid dynamics (CFD) analysis to determine permeability.

4.2. *Non-Darcian flow regime*

To evaluate the validity of the present results at higher Reynolds number, frictional losses in one row

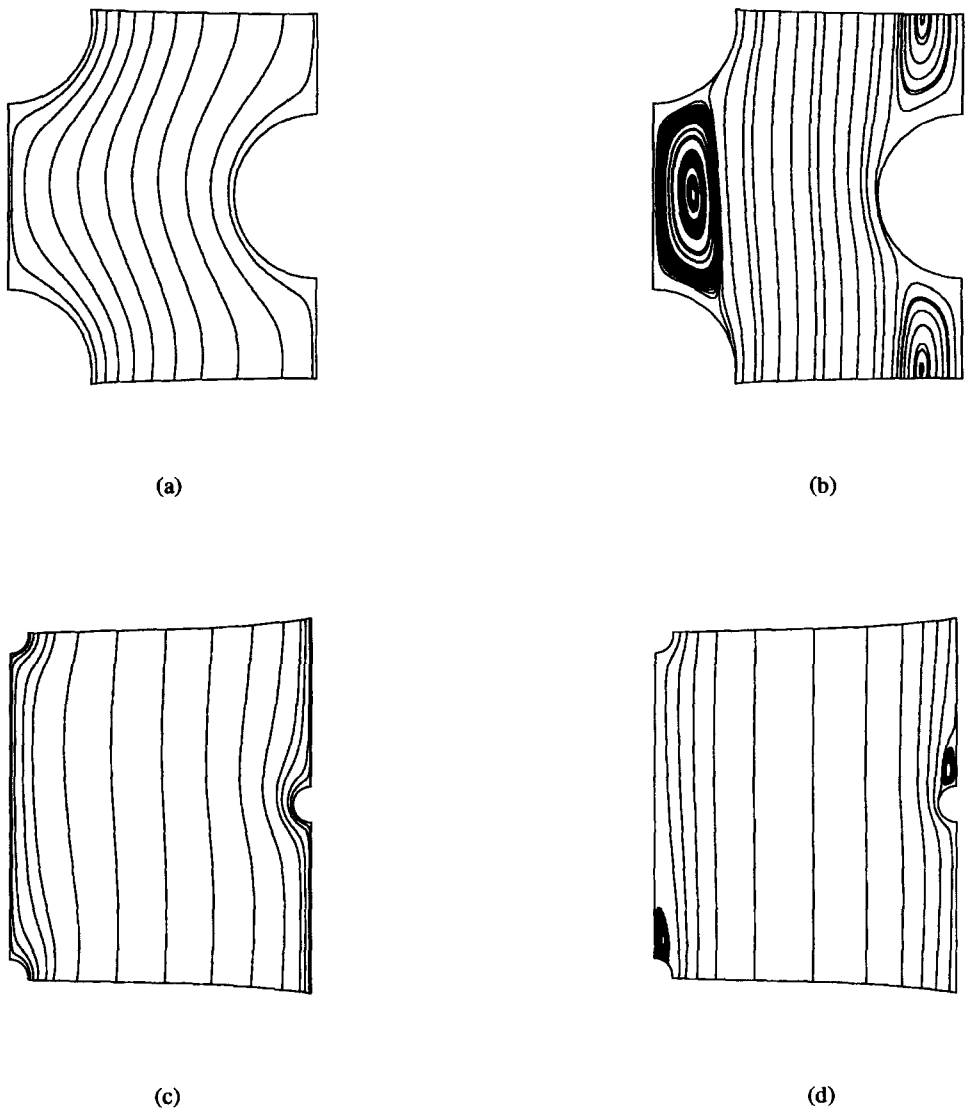

Fig. 3. Streamline plots for triangular array: (a) $\varepsilon_f = 0.80$, $Re_d = 3.01$ ($Re_{\sqrt{K}} = 0.849$); (b) $\varepsilon_f = 0.80$, $Re_d = 71.5$ ($Re_{\sqrt{K}} = 20.1$); (c) $\varepsilon_f = 0.99$, $Re_d = 3.89$ ($Re_{\sqrt{K}} = 12.4$); (d) $\varepsilon_f = 0.99$, $Re_d = 86.6$ ($Re_{\sqrt{K}} = 227$).

of a periodic array are compared against those reported in the literature. Figure 5 shows the non-dimensional pressure gradient vs. the particle Reynolds number for the square array with $\varepsilon_f = 0.80$. Two additional investigations, which are finite element-based numerical studies, are used for comparison: Edwards *et al.* [6]; and Ghaddar [8]. (Studies where $\varepsilon_f > 0.80$ could not be found in the literature for the Reynolds numbers considered.) There is good agreement between the present study and the other numerical results, especially at low Reynolds number. The larger difference at higher Reynolds number can be partly explained by unsteady effects. Ghaddar [8] performed a transient analysis and found inherently unsteady flows to exist for $Re_d > 150$ for this array. However, the relative percent difference in $-\nabla p^*$ between the present study and Ghaddar [8] (about 10%) suggests that unsteady effects are only slightly significant here.

Prior to the presentation of results for the full range of ε_f studied, the functional form of the pressure losses in porous media is considered in more detail. The pressure gradient $-\nabla\langle p_f\rangle^f$ for a given array can, in principle, be written as a function of the following variables: ρ, μ, $\langle v_f\rangle$, d, and K. The Buckingham–Pi theorem may be used to determine the non-dimensional groups that characterize this relationship: the Darcian Reynolds number $Re_{\sqrt{K}}$, the Darcy number Da, and the modified friction factor f', where

$$f' = -\nabla\langle p_f\rangle^f \frac{\sqrt{K}}{\rho\langle v_f\rangle \cdot |\langle v_f\rangle|}. \tag{19}$$

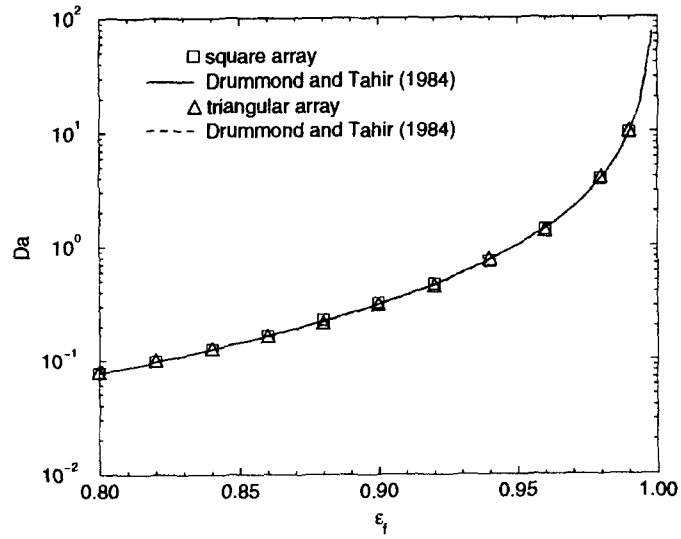

Fig. 4. Darcy number vs. fluid volume fraction for square and triangular arrays.

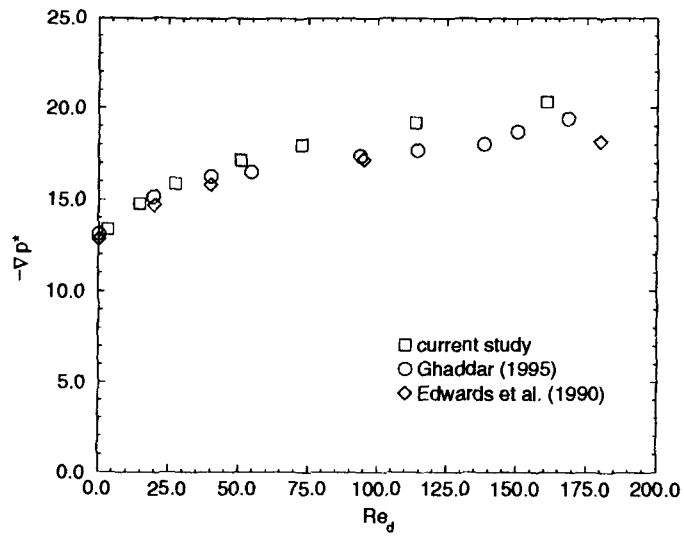

Fig. 5. Nondimensional pressure gradient vs. particle Reynolds number for square array, $\varepsilon_f = 0.80$.

Both the Ergun and Forchheimer relations can be rearranged to display the dependence of the frictional losses on these non-dimensional parameters. For example, the Forchheimer equation may alternatively be written as [14]

$$f' = 1/Re_{\sqrt{K}} + F. \tag{20}$$

(Ergun's equation may be written similarly.)

To examine the validity of the Ergun and Forchheimer relations, the modified friction factor is plotted vs. the Darcian Reynolds number for the square array and the triangular arrays in Fig. 6 on a logarithmic scale. Both Darcy's law and the Forchheimer relation are shown, with $F = 0.00251$ for the square array and 0.00412 for the triangular array. Several important features can be seen in this figure. First, the data reduces to the Darcy limit as $Re_{\sqrt{K}}$ approaches unity, as expected. However, the frictional losses clearly do not follow the Ergun and Forchheimer relations as the Darcian Reynolds number increases. The maximum relative difference between the present data and the Forchheimer relation is 25% for the square array and 66% for the triangular array. (It should be noted that the values for F were determined from the highest $Re_{\sqrt{K}}$ for each array type, since a linear regression yielded relative deviations well over 100%.) This finding calls into question the validity of the Forchheimer and Ergun expressions for flows in porous media composed of cylinder arrays. Previous studies [25] have shown that, for certain classes of porous media, the modified friction factor showed little dependence upon the fluid volume fraction. Cur-

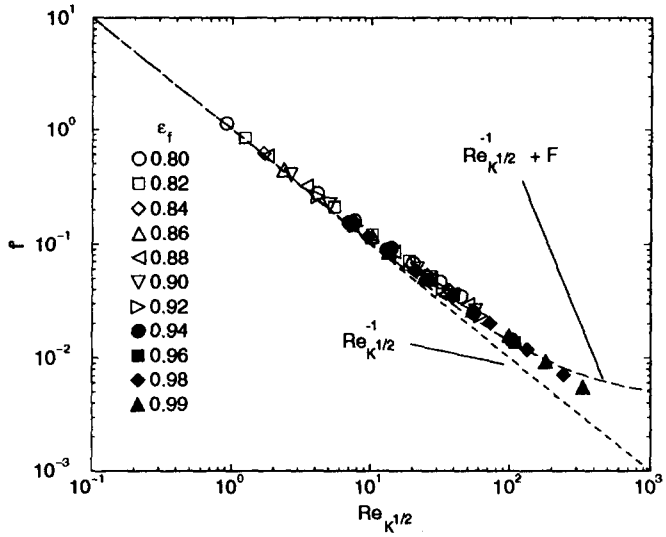

(a)

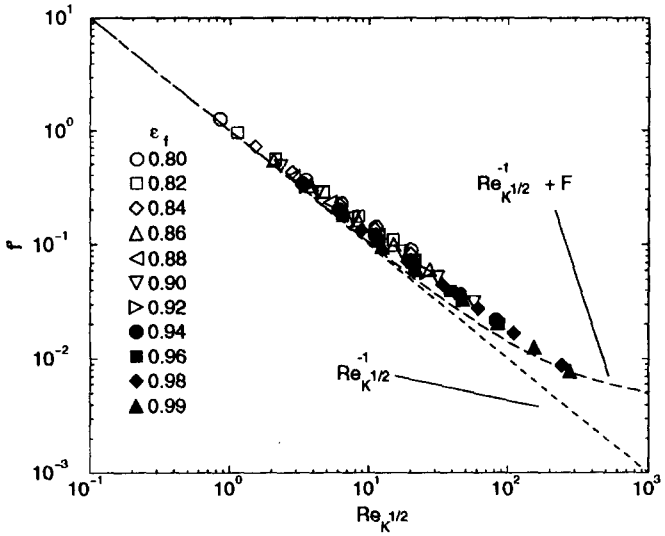

(b)

Fig. 6. Modified friction factor vs. Darcian Reynolds number: (a) square array; (b) triangular array.

rent results show that ε_f has a significant influence upon f', as shown by the scatter in the data points in this figure. To account for the fluid volume fraction dependency, a power-law relationship is proposed as the functional form of f' for $Re_{\sqrt{K}} > 1$:

$$f' = b\varepsilon_f^{-n} Re_{\sqrt{K}}^{m} \tag{21}$$

Figure 7 illustrates the fidelity of the above correlation for square and triangular arrays, respectively, by plotting $f'\varepsilon_f^n$ vs. $Re_{\sqrt{K}}$. The data matches the correlation to within a maximum relative difference of 6.5% for the square array and 4.5% for the triangular array. Values of the correlation constants are as follows: square array, $b = 0.862$, $m = -0.882$, and $n = 0.555$; triangular array, $b = 0.815$, $m = -0.836$, and $n = 1.21$. The larger value of n for the triangular array suggests a stronger dependence on fluid volume fraction, explained by the more tortuous flow path of this

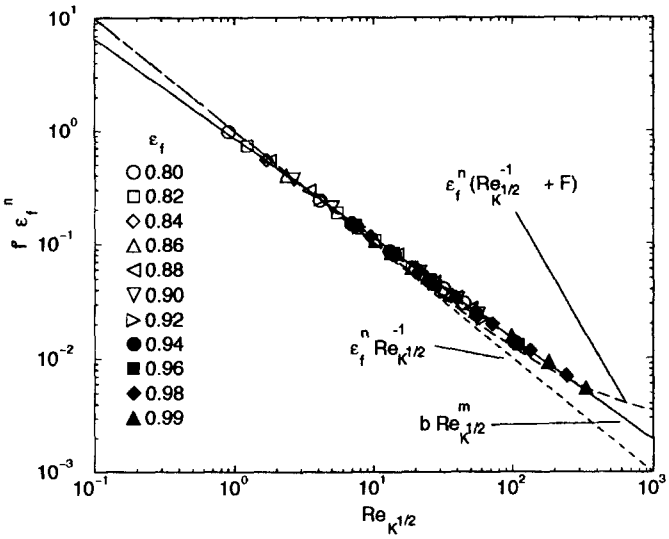

(a)

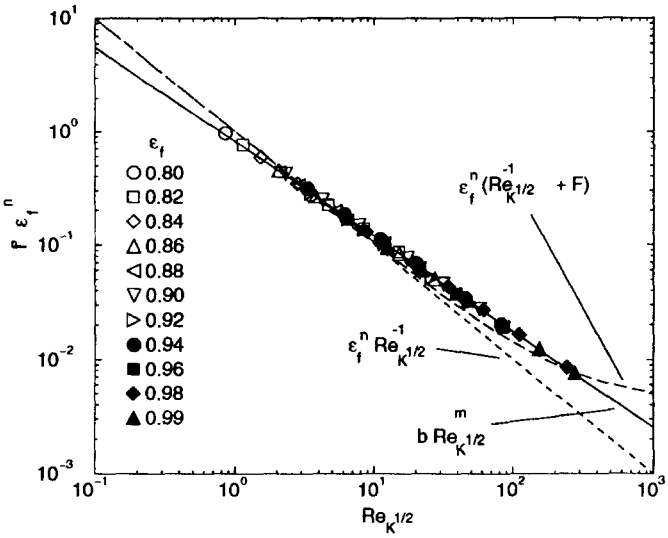

(b)

Fig. 7. Modified friction factor as a function of fluid volume fraction, vs. Darcian Reynolds number: (a) square array; (b) triangular array.

array type. For the triangular array, the tortuosity of the flow path is greatly exacerbated by a decrease in porosity, while a more open flow area exists for the square array. Hence, f' shows more sensitivity to the fluid volume fraction for the triangular array. Both arrays show comparable dependency upon $Re_{\sqrt{K}}$, although the modified friction factor is higher for the triangular array for the reasons outlined above.

5. RESULTS: HEAT TRANSFER

Heat transfer effects are seen in Figs. 8 and 9, which show isotherms for square and triangular arrays con-

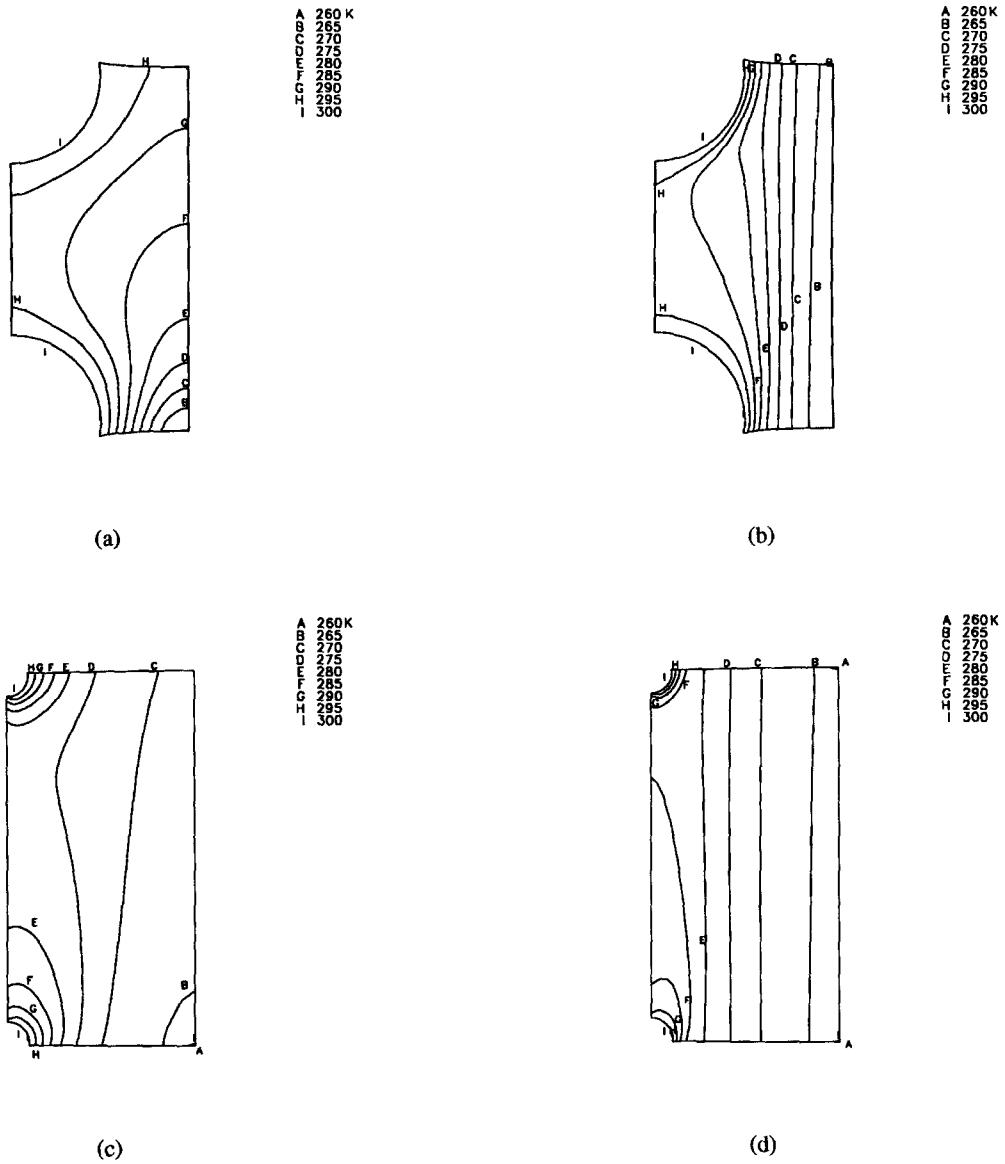

Fig. 8. Isotherm plots for square array, $\langle T_s \rangle^s = 300$ K: (a) $\varepsilon_f = 0.80$, $Re_d = 3.26$ ($Re_{\sqrt{K}} = 0.904$); (b) $\varepsilon_f = 0.80$, $Re_d = 161$ ($Re_{\sqrt{K}} = 44.6$); (c) $\varepsilon_f = 0.99$, $Re_d = 4.24$ ($Re_{\sqrt{K}} = 13.3$); (d) $\varepsilon_f = 0.99$, $Re_d = 105$ ($Re_{\sqrt{K}} = 331$).

sidering extreme values of fluid volume fraction and Reynolds number. The isotherms display symmetric shapes for low Reynolds number flows, showing the dominance of conduction over convection. At high Reynolds numbers, isotherms in open flow areas are aligned parallel to the y-axis, with more complicated patterns appearing in the recirculation zones. Also, much sharper temperature gradients appear closer to the cylinders as the Reynolds number increases.

To evaluate convective heat transfer, the Nusselt number Nu_d is defined as

$$Nu_d = \frac{h_{fs} d}{k}. \tag{22}$$

The convective heat transfer coefficient h_{fs} is determined from equation (12), with $T_s = \langle T_s \rangle^s$ and $T_r = \langle T_f \rangle^f$. (It should be noted that T_r is conventionally taken as the fluid bulk temperature; however, $\langle T_f \rangle^f$ is chosen for convenience. Calculations of the Nusselt number based on the bulk temperature revealed only small differences.) For the case of constant wall temperature, q_s'' is found via an energy balance between the inlet and outlet of the fluid domain and the cylinder walls. Figure 10 shows the Nusselt number vs. the particle Reynolds number for both array types ($\langle T_s \rangle^s = 300$ K for constant wall temperature, and $q_s'' = 2.12 \times 10^{-4}$ W m^{-2} for constant wall heat flux). The fluid volume fraction clearly has

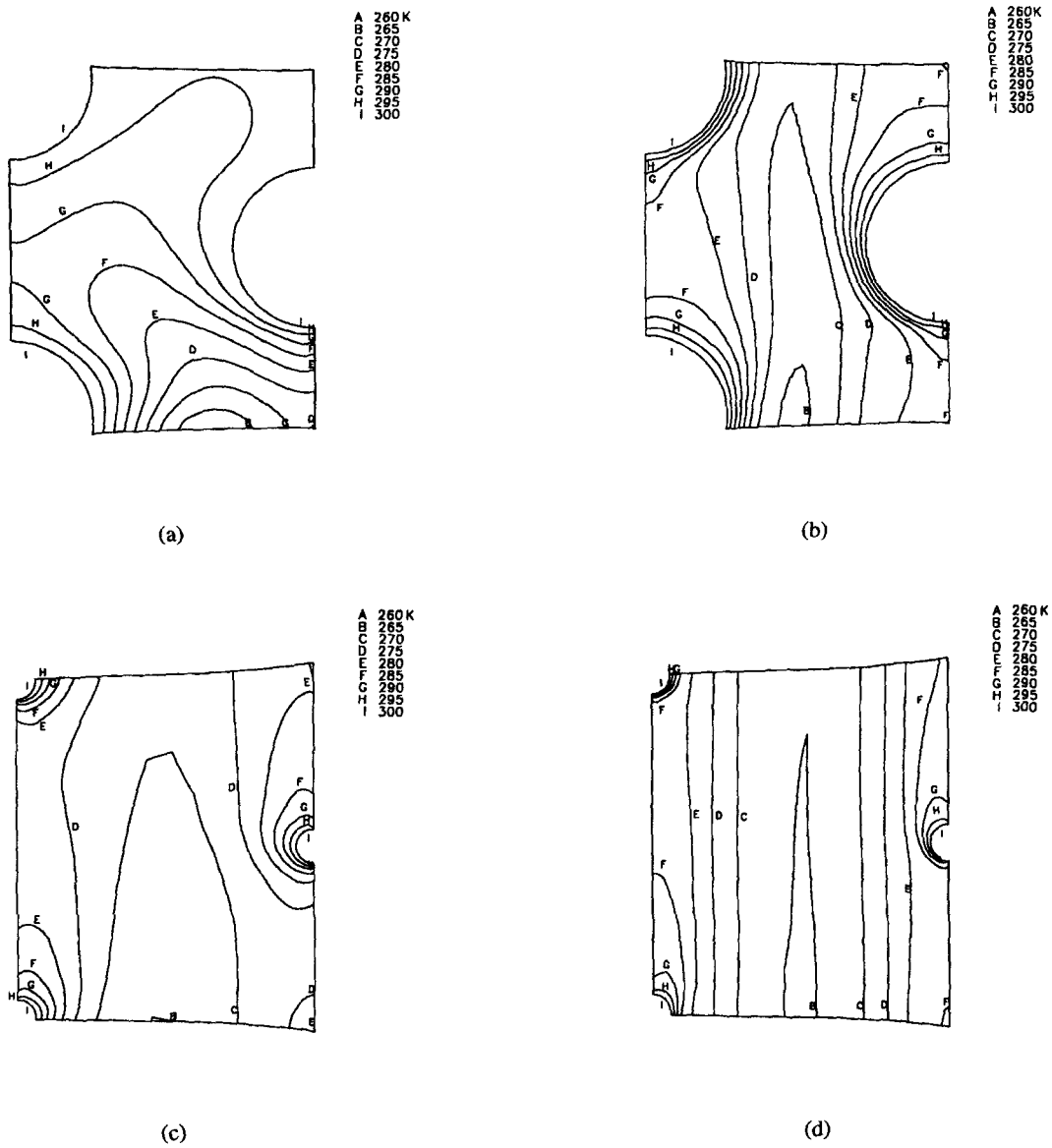

Fig. 9. Isotherm plots for triangular array, $\langle T_s \rangle^s = 300$ K: (a) $\varepsilon_f = 0.80$, $Re_d = 3.01$ ($Re_{\sqrt{K}} = 0.849$); (b) $\varepsilon_f = 0.80$, $Re_d = 71.5$ ($Re_{\sqrt{K}} = 20.1$); (c) $\varepsilon_f = 0.99$, $Re_d = 3.89$ ($Re_{\sqrt{K}} = 12.4$); (d) $\varepsilon_f = 0.99$, $Re_d = 86.6$ ($Re_{\sqrt{K}} = 277$).

a strong influence on the degree of heat transfer, as Nu_d rises when the cylinders are closer to each other. There is also a marked dependency upon the wall heating condition, with the constant wall heat flux condition exhibiting Nusselt numbers that are about 20% higher than the constant wall temperature case. A power-law correlation is used as a fit for the data,

$$Nu_d = g\, Re_d^r. \tag{23}$$

This correlation is considered to be a first approximation, as the results show that the values of coefficients g and r are not independent of Re_d. Table 2 lists the coefficients for the square and triangular arrays as a function of the fluid volume fraction for each heating condition (δ_m is the maximum relative difference).

The relatively moderate values of the Nusselt number suggest that departure from LTE may be significant in those cases where non-equilibrium effects are suspected. However, it is not possible to generally assess the importance of the LTE assumption from the Nusselt number alone, since the interfacial area a_{fs} can attain very large values even for high porosities. Macroscopic analyses similar to the investigation of Amiri and Vafai [12], along with the Nusselt number correlations presented herein, can be used to assess

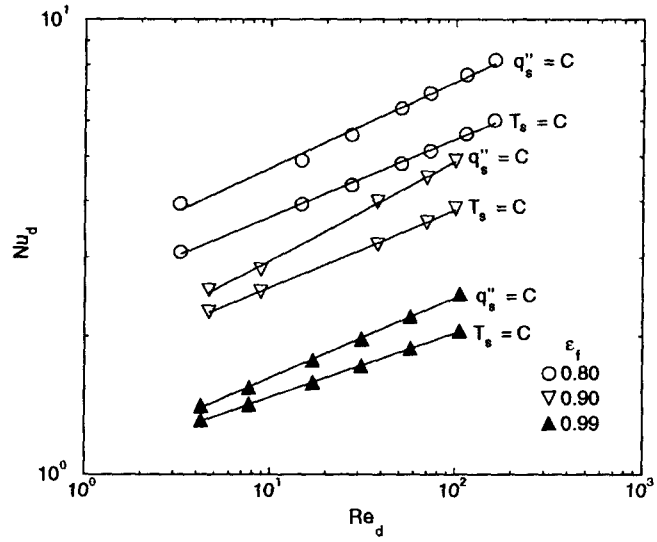

(a)

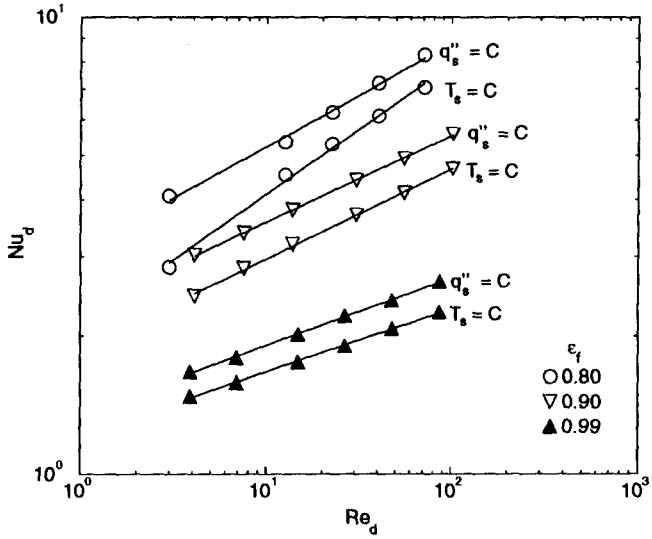

(b)

Fig. 10. Nusselt number vs. particle Reynolds number: (a) square array; (b) triangular array.

LTE for flows in porous media consisting of cylinder arrays.

Finally, it should be noted that an attempt was made to utilize $\sqrt{K}$ as a length scale of heat transfer in order to determine if the data could be represented as a function of the Darcian Reynolds number or as a Nusselt number based on $\sqrt{K}$. While application of the Buckingham–Pi theorem to heat transfer reveals dependency on dimensionless groups Re_d, Nu_d, and Da, there is no guarantee that the functional relationship is analogous to that found for the modified friction factor. This attempt yielded no conclusive evidence of universal behavior in the Nusselt number as a function of the fluid volume fraction. Hence, the results have been presented in the more traditional fashion with the cylinder diameter as the length scale.

Table 2. Correlation values for Nusselt number: (a) square array; (b) triangular array

ε_f	$T_s = C$			$q_s'' = C$		
	g	r	δ_m (%)	g	r	$\lvert\delta_m\rvert$ (%)
			(a)			
0.80	2.50	0.170	1.4	3.05	0.191	3.8
0.82	2.38	0.166	1.0	2.78	0.192	3.1
0.84	2.21	0.169	1.2	2.47	0.204	2.3
0.86	2.04	0.171	0.8	2.19	0.212	1.4
0.88	1.87	0.174	0.9	2.03	0.210	2.2
0.90	1.73	0.172	0.7	1.79	0.218	1.9
0.92	1.60	0.167	0.4	1.57	0.221	1.0
0.94	1.46	0.162	0.6	1.37	0.227	0.7
0.96	1.35	0.147	0.2	1.26	0.207	0.9
0.98	1.18	0.138	0.3	1.13	0.193	1.7
0.99	1.07	0.140	0.5	1.08	0.177	1.2
			(b)			
0.80	2.12	0.286	3.0	3.11	0.226	3.1
0.82	2.12	0.268	1.9	2.87	0.226	1.8
0.84	2.10	0.245	1.4	2.70	0.221	1.1
0.86	2.06	0.225	1.0	2.46	0.224	1.2
0.88	2.00	0.209	0.7	2.16	0.256	2.2
0.90	1.89	0.196	1.2	2.31	0.189	0.7
0.92	1.81	0.176	0.5	2.17	0.175	0.2
0.94	1.68	0.162	0.4	2.01	0.163	0.8
0.96	1.54	0.146	0.3	1.80	0.154	0.7
0.98	1.34	0.143	1.2	1.56	0.150	1.2
0.99	1.21	0.138	0.8	1.35	0.150	0.6

6. SUMMARY AND CONCLUSIONS

Frictional losses in sparse, periodic arrays follow Darcy's law when the Darcian Reynolds number is of the order one, but show significant non-Darcy effects as the Reynolds number increases. Comparison to previous numerical studies in square arrays reveal few differences, especially at low Reynolds number. The modified friction factor is shown to follow a power-law function of Darcian Reynolds number rather than the Ergun or Forchheimer relations, with strong dependency on the fluid volume fraction. Nusselt number correlations utilizing the cylinder diameter as the length scale are also derived via a power-law relationship. Findings from the current investigation suggest that additional studies are merited for flows in highly porous media, owing to the reported departure from the Ergun and Frochheimer relations. In particular, investigations should be conducted which consider transitional and/or turbulent flows, since their existence will greatly impact the flow field at higher Reynolds number.

REFERENCES

1. Åström, B., Pipes, R. and Advani, S., On flow through aligned fiber beds and its application to composites processing. *Journal of Composite Materials*, 1992, **26**(9), 1351–1373.
2. Žukauskas, A., Heat transfer from tubes in crossflow. *Advances in Heat Transfer*, 1987, **18**, 87–159.
3. Žukauskas, A., Convective heat transfer in cross flow. In *Handbook of Single-Phase Convective Heat Transfer*, ed. S. Kakaç, R. K. Shah and W. Aung, Chap. 6. Wiley, New York, 1987.
4. Drummond, J. and Tahir, M., Laminar viscous flow through regular arrays of parallel solid cylinders. *International Journal of Multiphase Flow*, 1984, **10**(5), 515–540.
5. Sangani, A. S. and Acrivos, A., Slow flow past periodic arrays of cylinders with application to heat transfer. *International Journal of Multiphase Flow*, 1982, **8**(3), 193–206.
6. Edwards, D. A., Shapiro, M., Bar-Yoseph, P. and Shapira, M., The influence of Reynolds number upon the apparent permeability of spatially periodic arrays of cylinders. *Physics of Fluids*, 1990, **2**(1), 45–55.
7. Eidsath, A., Carbonell, R. G., Whitaker, S. and Herrmann, L. R., Dispersion in pulsed systems—III. Comparison between theory and experiments for packed beds. *Chemical Engineering Science*, 1983, **38**(11), 1803–1816.
8. Ghaddar, C. K., On the permeability of unidirectional fibrous media: a parallel computational approach. *Physics of Fluids*, 1995, **7**(11), 2563–2586.
9. Im, K. H. and Ahluwalia, R. K., Radiative enhancement of tube-side heat transfer. *International Journal of Heat and Mass Transfer*, 1994, **37**(17), 2635–2646.
10. Hendricks, R. C., Braun, M. J., Canacci, V. and Mullen, R. L., Simulation of brush insert for leading-edge-passage convective heat transfer. In *Fourth International Symposium in Transport Phenomena*, Sydney, 1991.
11. Žukauskas, A. and Ulinskas, R., Banks of plain and finned tubes. In *Hemisphere Handbook of Heat Exchanger Design*, ed. G. F. Hewitt, Chap. 2.2.4. Hemisphere, New York, 1990.
12. Amiri, A. and Vafai, K., Analysis of dispersion effects and non-thermal equilibrium, non-Darcian, variable porosity incompressible flow through porous media. *International Journal of Heat and Mass Transfer*, 1994, **37**(6), 939–954.
13. Vafai, K. and Sözen, M., Analysis of energy and momentum transport for fluid flow through a porous bed. *Journal of Heat Transfer*, 1990, **112**, 690–699.

14. Bejan, A., *Convective Heat Transfer*. Wiley-Interscience, New York, 1984.
15. Cheng, P., Heat transfer in geothermal systems. *Advances in Heat Transfer*, 1978, **14**, 1–105.
16. Bauer, T., A general analytical approach toward thermal conductivity of porous media. *International Journal of Heat and Mass Transfer*, 1993, **36**(17), 4181–4191.
17. Shyy, W., Thakur, S., Ouyang, H., Liu, J. and Blosch, E., *Computational Techniques for Complex Transport Phenomena*. Cambridge University Press, New York, 1997.
18. Ergun, S., Fluid flow through packed columns. *Chemical Engineering Progress*, 1952, **48**(2), 89–94.
19. Bear, J., *Dynamics of Fluids in Porous Media*. Dover, New York, 1988.
20. Thakur, S., Wright, J., Shyy, W., Liu, J., Ouyang, G. and Vu, T., Development of pressure-based composite multigrid methods for complex fluid flows. *Progress in Aerospace Sciences*, 1996, **32**, 313–375.
21. Shyy, W., *Computational Modeling for Fluid Flow and Interfacial Transport*. Elsevier Science Publishers, Amsterdam, 1994.
22. Patankar, S. V., *Numerical Heat Transfer and Fluid Flow*. Hemisphere, New York, 1980.
23. Patankar, S. V., Liu, C. H. and Sparrow, E. M., Fully developed flow and heat transfer in ducts having streamwise-periodic variations of cross-sectional area. *Journal of Heat Transfer*, 1977, **99**, 180–186.
24. Incropera, F. and DeWitt, D., *Fundamentals of Heat and Mass Transfer*, 2nd edn. Wiley, New York, 1985.
25. Beavers, G. and Sparrow, E., Non-Darcy flow through fibrous porous media. *Journal of Applied Mechanics*, 1969, **36**, 711–714.